

**UCC Library and UCC researchers have made this item openly available.
 Please [let us know](#) how this has helped you. Thanks!**

Title	Size controlled synthesis of silicon nanocrystals using cationic surfactant templates
Author(s)	Linehan, Keith; Doyle, Hugh
Publication date	2013-09-11
Original citation	LINEHAN, K. & DOYLE, H. 2014. Size Controlled Synthesis of Silicon Nanocrystals Using Cationic Surfactant Templates. <i>Small</i> , 10, pp. 584-590. doi: 10.1002/sml.201301189
Type of publication	Article (peer-reviewed)
Link to publisher's version	http://dx.doi.org/10.1002/sml.201301189 Access to the full text of the published version may require a subscription.
Rights	© 2013, John Wiley & Sons, Inc. This is the peer reviewed version of the following article: LINEHAN, K. & DOYLE, H. 2014. Size Controlled Synthesis of Silicon Nanocrystals Using Cationic Surfactant Templates. <i>Small</i> , 10, pp. 584-590, which has been published in final form at http://dx.doi.org/10.1002/sml.201301189 . This article may be used for non-commercial purposes in accordance with Wiley Terms and Conditions for Self-Archiving. http://olabout.wiley.com/WileyCDA/Section/id-820227.html#terms
Item downloaded from	http://hdl.handle.net/10468/2514

Downloaded on 2021-05-08T20:22:24Z

DOI: 10.1002/sml.((please add manuscript number))

Size Controlled Synthesis of Silicon Nanocrystals using Cationic Surfactant Templates

*Keith Linehan and Hugh Doyle**

K. Linehan, H. Doyle
Tyndall National Institute
University College Cork
Lee Maltings
Cork
Ireland
E-mail: hugh.doyle@tyndall.ie

Supporting Information is available on the WWW under <http://www.small-journal.com> or from the author.

Keywords: silicon nanocrystals, synthesis, inverse micelle, photoluminescence, quantum yield

Alkyl-terminated silicon nanocrystals (Si NCs) are synthesized at room temperature by hydride reduction of silicon tetrachloride (SiCl_4) within inverse micelles. Highly monodisperse Si nanocrystals with average diameters ranging from 2 to 6 nm are produced by variation of the cationic quaternary ammonium salts used to form the inverse micelles. Transmission electron microscopy (TEM) imaging shows that the NCs are highly crystalline, while FTIR spectra confirm that the NCs are passivated by covalent attachment of alkanes, with minimal surface oxidation. UV-Visible absorbance (UV-Vis) and photoluminescence spectroscopy (PL) show significant quantum confinement effects, with moderate absorption in the UV spectral range, and a strong blue emission with a marked dependency on excitation wavelength. The photoluminescence quantum yield (Φ) of the Si NCs exhibits an inverse relationship with the mean NC diameter, with a maximum of 12 % recorded for 2 nm NCs.

1. Introduction

Semiconductor nanocrystals (NCs) or quantum dots have been extensively studied over the last 25 years since their size-dependent optical and electronic properties make them useful materials in applications ranging from biological imaging to optoelectronic devices.^[1] More recently, research interest in the preparation of size monodisperse, oxide-free silicon NCs (Si NCs) has been steadily increasing, as the momentum requirements due to the indirect band gap structure of bulk Si are relaxed in the 1–5 nm size range as a result of quantum confinement effects.^[2] This allows for the excellent optical and electronic properties typical of group III-V and II-VI materials, such as size-tunable and narrow luminescence and high quantum yields, to be combined with the richness of silicon surface chemistry. In addition, group IV materials such as silicon are also nontoxic, highly abundant, biocompatible, electrochemically stable, and compatible with standard CMOS processing methods used by the microelectronics industry.

A large variety of both physical and chemical methods have been reported for the preparation of Si NCs, including physical and chemical vapor deposition,^[3] thermal annealing,^[4] laser induced-heating of gaseous precursors,^[5] electrochemical etching of crystalline silicon wafers,^[6] thermal decomposition of silane precursors^[7] and the reduction of silicon halides by various reducing agents.^[8,9] The use of inverse micelle templates for preparation of a wide range of nanocrystals such as metals, and semiconductor materials has been widely reported, as the nucleation and growth kinetics of both 0-D and 1-D nanostructures may be controlled depending on the molecular structure of the surfactant and reaction conditions used.^[10] The preparation of Si NCs by reduction of silicon halide by LiAlH_4 within inverse micelles was first reported by Wilcoxon *et al.*, which resulted in 2 – 10 nm Si NCs with hydrogenated surfaces.^[11] This method was later refined by Tilley and co-workers, who improved the

stability of the as-synthesized nanoparticles by further modification of the nanocrystal surface using a Pt-catalyzed hydrosilylation process to form chemically robust Si–C bonds on the surface.^[12] This surface modification strategy both chemically passivates the nanocrystal surface to prevent oxidation, and allows for Si NCs to be derivatized with a variety of surface functionalities.^[13,14] More recently, alkyl trichlorosilanes have been utilized as both reductant and ligand, resulting in formation of both alkyl- and alkene-functionalized Si NCs.^[15] While microemulsion synthesis methods for preparation of high quality, size monodisperse Si NCs are well established, to the best of our knowledge, no studies have been carried out on the effect of the surfactant structure in determining the size and shape the resultant Si NCs. Here we report a simple method for the size controlled synthesis of Si NCs within inverse micelles having well defined core diameters ranging from 2 to 6 nm. Regulation of the Si NCs size was achieved by variation of the cationic quaternary ammonium salts used to form the inverse micelles. Through controlling the size of the nanocrystals, their resulting photoluminescence properties could be tuned.

2. Results and Discussion

Alkyl-terminated Si NCs were synthesized by room temperature reduction of silicon tetrachloride by lithium aluminum hydride under inert atmosphere; see Experimental Section for further details. Figure 1 shows low magnification transmission electron microscope (TEM) images of Si NCs prepared in the presence of the cationic quaternary ammonium salts tetraoctyl ammonium bromide (TOAB), tetrabutyl ammonium bromide (TBAB), cetyltrimethyl ammonium bromide (CTAB), didodecyldimethyl ammonium bromide (DDAB), dodecyltrimethyl ammonium bromide (DTAB) and tetradodecyl ammonium bromide (TDAB), see Figure S.1 of the Supporting Information for chemical structures of these surfactants. TEM imaging of Si NCs synthesized in the presence of TOAB as the surfactant template (Figure 1(a)) show that the Si NCs are highly size and shape monodisperse, with no evidence

of aggregation. Inset in Figure 1(a) is a histogram of NC diameters, determined by analysis of TEM images of *ca.* 200 NCs located at random locations on the grid. Fitting the histogram to a Gaussian model yielded a mean diameter of 1.9 nm, with a standard deviation of 0.3 nm, closely matching with the (111) interplanar spacing of bulk silicon, emphasizing the highly size monodisperse nature of the NCs. This is in good agreement with reports published by both Tilley^[12] and Zuilhof^[16] and co-workers, who used TOAB as the surfactant for the synthesis of Si NCs. Replacing TOAB with either TBAB and CTAB resulted in an increase in the mean NC diameter to 2.5 ± 0.3 nm and 2.6 ± 0.3 nm respectively, without a concomitant increase in size dispersity, see Figures 1(b) and 1(c). Si NCs synthesized in the presence of DDAB (3.0 nm) and DTAB (4.0 nm) were found to be larger in size and more irregular in shape, with a standard deviation of 0.9 nm, see Figures 1(d-e). The largest NCs (5.8 ± 1.8 nm) were obtained when TDAB was employed as the surfactant, though this was accompanied by a significant increase in size and shape polydispersity.

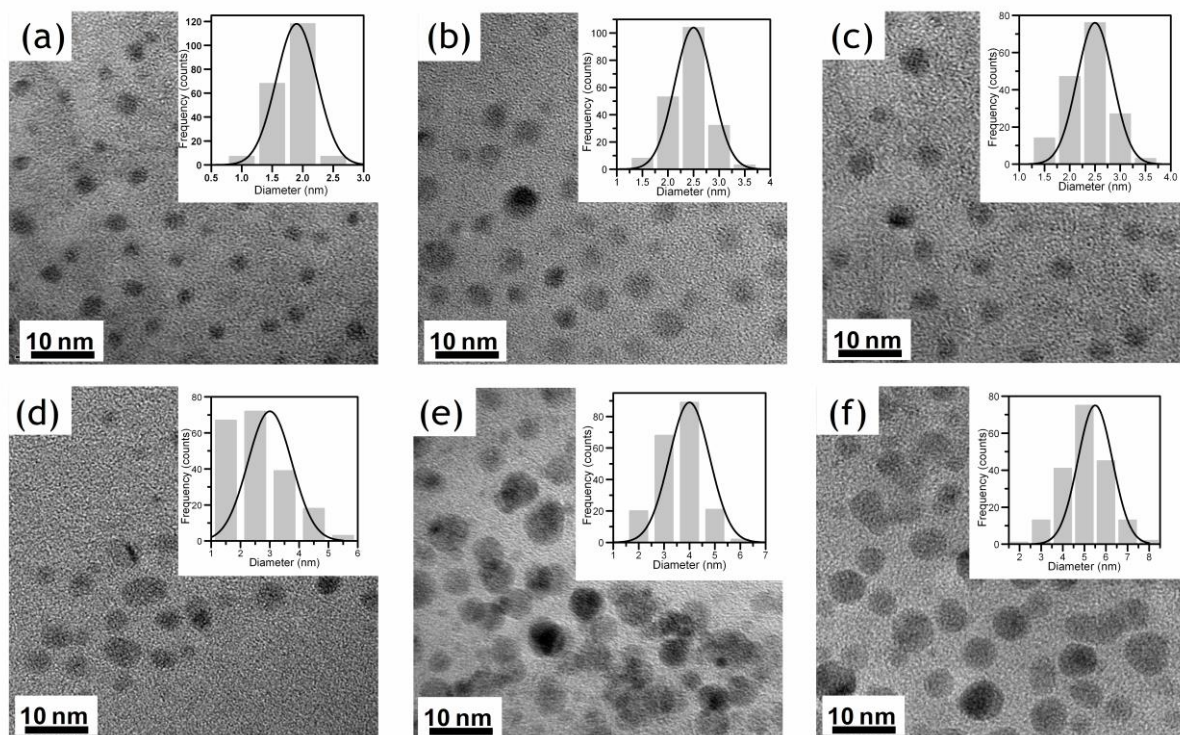


Figure 1. Representative TEM images of the Si NCs synthesized in the presence of the following surfactants: a) TOAB, b) TBAB, c), CTAB, d) DDAB, e) DTAB, and f) TDAB. Inset: Size histograms of the Si NCs with curves fit to the data using a Gaussian model.

High-resolution TEM (HR-TEM) imaging was used in conjunction with selective area diffraction (SAED) to confirm the crystallinity and establish the crystal phase of the as-synthesized NCs; see Figures 2(a-b)), respectively. HR-TEM imaging of Si NCs produced using DTAB (Figure 2(a)) as the surfactant showed that the Si NCs form a single contiguous crystalline phase, without the presence of packing defects. The lattice fringes shown in Figure 2(a) correspond to a d spacing of 1.2 Å, matching the (331) spacing reported for the silicon unit cell. Selected area diffraction (SAED) patterns of the Si NCs, see Figure 2(b), shows rings consistent with the diamond lattice of Si; (111) at 3.14 Å, (200) at 1.92 Å, (311) at 1.68 Å and (400) at 1.31 Å, see Supporting Information, Table S.1. Figure 2(c) shows the energy dispersive X-ray (EDX) spectrum, where the Si peak corresponding to the presence of the NCs is evident. Other elemental peaks assigned to the presence Cl and Ca are probably due to solvent artefacts, while the Cu peaks are due to the carbon-coated copper grid.

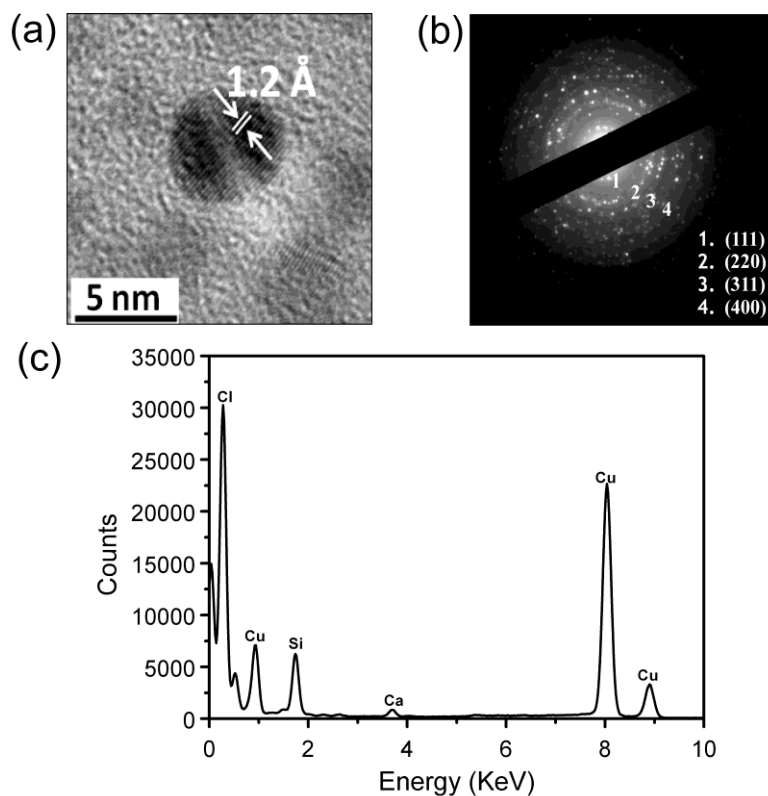


Figure 2. a) HR-TEM, b) SAED pattern, and c) EDX profile of the silicon nanocrystals synthesized with DTAB as the surfactant.

The surface chemistry of the Si NCs was characterized by infrared spectroscopy (see Figure S.2, Supporting Information) to identify the terminal moieties on the nanocrystal surface. Figure S.2 (see Supporting Information) shows the spectrum obtained for Si NCs synthesized using TOAB as the surfactant, although similar spectra were obtained for all the nanocrystals reported here. The Si NCs exhibit clear C-H stretching signals, with symmetric CH₂, asymmetric CH₂, and the asymmetric C-CH₃ stretching vibrations at 2856, 2926, and 2959 cm⁻¹, respectively. The peak at 1378 cm⁻¹ is assigned to the C-CH₃ symmetrical bending mode, while the peaks at 1260 and 1460 cm⁻¹ are attributed to the symmetric bending and scissoring vibration of the Si-C bond, respectively. The absence of the CH=CH₂ peaks at 1640 and 3080 cm⁻¹, combined with the formation of the Si-C bond at 1460 cm⁻¹, confirms covalent attachment of the 1-heptene to the NC surface.^[3,12,16] The absence of peaks between 1000–1100 cm⁻¹, corresponding to Si-OR stretching vibrations, highlights that the silicon nanocrystals are well passivated, with minimal surface oxidation.

The surface chemistry of the Si NCs was also investigated by using high resolution XPS spectroscopy, see Figure S.3 of the Supporting Information. The Si 2p spectra in Figure S.3(a) shows a strong peak centered at 102.2 eV, in good agreement with previous reports for alkyl-capped silicon nanocrystals.^[17] The main peak at 102.2 eV is assigned to Si-C bonding, confirming covalent attachment of alkyl groups to the Si NC surface, while the presence of the peak at 103.0 eV is indicative of some surface oxidation (Si-O_x) that was not observed in the FTIR spectrum (Figure S.2). The C1s spectrum in Figure S.3(b) has a strong at 284.8 eV, assigned to C-C bonding, and two minor peaks at 284.1 and 285.6 eV are assigned to C-C/C-H and C-O bonding, respectively. The existence of a Si-C component agrees with the FTIR spectra indicating covalent attachment of the alkyl ligands to the nanocrystal surface. The O1s

spectrum in the Figure S.3(c) is fitted with two components at binding energies of 532.2 and 533.0 eV, assigned to the presence of Si–O_x groups at the nanocrystal surface.

Figure 3 shows the UV-Vis absorption spectra of the silicon nanocrystals in hexane prepared using the different surfactants. The spectrum of the smallest nanocrystals (1.9 nm), synthesized when TOAB was employed as the surfactant, showed a broad absorption band centered at *ca.* 260 nm with an onset of absorbance located at 350 nm. This is in excellent agreement with previous reports for similarly sized alkyl-terminated Si NCs, which have assigned this feature to the direct Γ - Γ band gap transition.^[11,18] Increasing the mean NC diameter to *ca.* 2.5 nm by using TBAB or CTAB as the surfactant resulted in a distinct red-shift in the wavelength position of the absorption band to 266 and 267 nm, respectively. Further red shifts in the absorption spectrum were observed for increasing nanocrystal sizes, with the largest size nanocrystals (5.8 nm) showing a strong peak centered at 272 nm, corresponding to a 12 nm shift compared to the smallest (1.9 nm) nanocrystals. Interestingly, the changes in size distribution do not significantly affect the onset of absorbance, located at *ca.* 350 nm (3.5 eV), which is considerably blue shifted from that of bulk silicon.

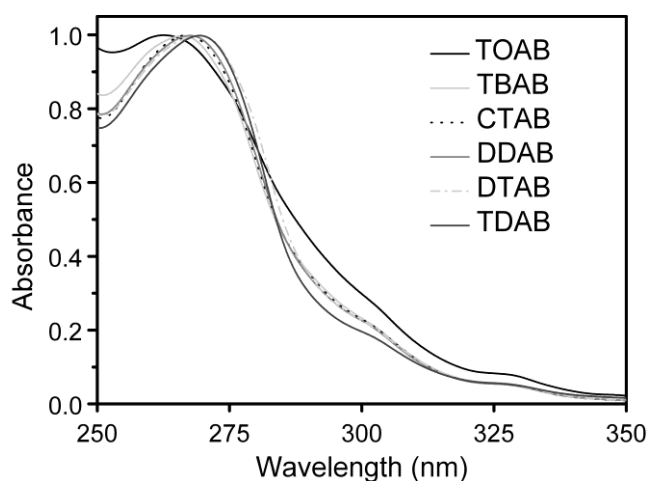


Figure 3. Normalized UV-Vis absorption spectra of the silicon nanocrystals synthesized in the presence of the various surfactants.

The absence of vibrational features in the absorption spectra, which have been observed for Si NCs prepared using a similar approach and assigned to the presence of trace amounts of toluene,^[19] indicates the utility of the column chromatography purification of the as-synthesized nanocrystals,^[9] see Experimental Section and Figure S.4 of the Supporting Information for further details.

Figure 4 shows the photoluminescence (PL) spectra (280 nm excitation) of the Si NCs synthesized using the different surfactants measured at room temperature. Dilute dispersions of the Si NCs in hexane were prepared with the same optical densities for comparison. Luminescence from the Si NC dispersions is observed over a narrow spectral range between 300 – 420 nm, with a wavelength maximum at *ca.* 330 nm, similar to that reported for other alkyl terminated silicon nanocrystals.^[12,20,21] The full width at half maximum (FWHM) was found to be *ca.* 60 nm, emphasizing the monodispersity of the nanocrystals.^[12] While the luminescence intensity decreases monotonically with increasing nanocrystal diameter, there is no change in the PL spectra of the Si NCs for with core diameters ranging from 2 to 6 nm.

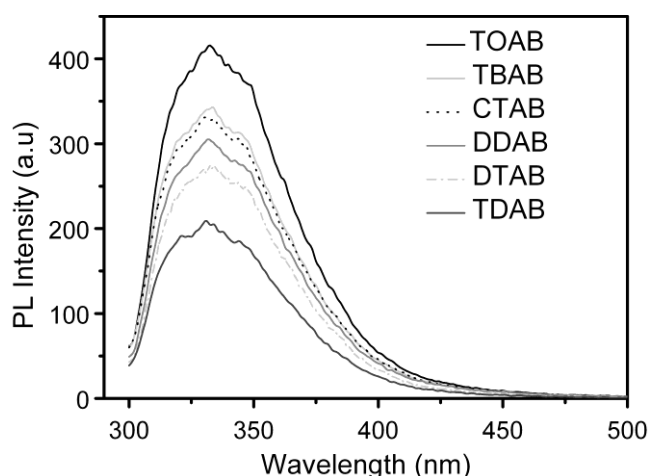


Figure 4. Photoluminescence spectra of the silicon nanocrystals synthesized in the presence of the various surfactants. Spectra were recorded on samples with the same optical density at an excitation wavelength of 280 nm.

Despite extensive investigation over the last 10-15 years, the exact origin of PL from nanocrystalline silicon remains a divisive topic, complicated by presence of both direct and indirect band gap transitions.^[14,22] The wide variety of synthetic strategies reported, together with broad particle size distributions, different ligand passivation schemes and surface oxidation, have all contributed to the lack of consensus.^[22,23] The underlying mechanism is usually described in terms of either a quantum confinement model based on quantum size effects in the nanocrystalline silicon core, or a surface chemistry model that emphasizes the importance of surface phenomena at the interface between the crystalline core and the host matrix.^[24] Both models present extreme viewpoints, and other theories combining elements of both models have also been presented.^[25] The marked size dependency observed in the UV-Vis absorption spectra shown in Figure 3 agrees well with the quantum confinement model, supporting the assignment to direct transitions within the nanocrystal core. In contrast, the PL spectra shown in Figure 4 exhibit a blue emission that is independent of nanocrystals, implying that exciton recombination is not confined within the nanocrystal core, and that the nanocrystal surface must be involved in the emission process. The uniformity of the luminescence observed from Si NCs (the normalized PL spectra are entirely superimposable) suggests that a limited number of surface or near-interface states are involved. This interpretation is in agreement with studies on hydrogen-terminated Si NCs by Yang *et al.*, who concluded the most plausible mechanism is that excitons are first formed within Si NCs by direct transitions at Γ or X point, which transfer to and recombine at states close to the interface between the nanocrystal and the surrounding matrix.^[25] Further evidence for the role of surface states in the luminescence process was recently provided by Dasog *et al.*,^[20] who demonstrated tuning of the emission color of Si NCs from red to blue by titration with trace amounts of nitrogen-containing compounds.

Figure 5(a) shows the photoluminescence spectra of TOAB-synthesized 1.9 nm Si NCs in hexane, obtained using excitation wavelengths ranging from 280 to 400 nm in 20 nm intervals. The photoluminescence spectra display small features within the main peak at different excitation wavelengths, in agreement with previous results.^[18] Excitation energies for maximum PL intensity (4.4 eV) significantly exceed the absorption edge (3.5 eV), with PL intensity that depends sensitively on excitation energy. The wavelength position of the PL maximum ranges from 330 nm for excitation at 280 nm, to 438 nm for 400 nm excitation.

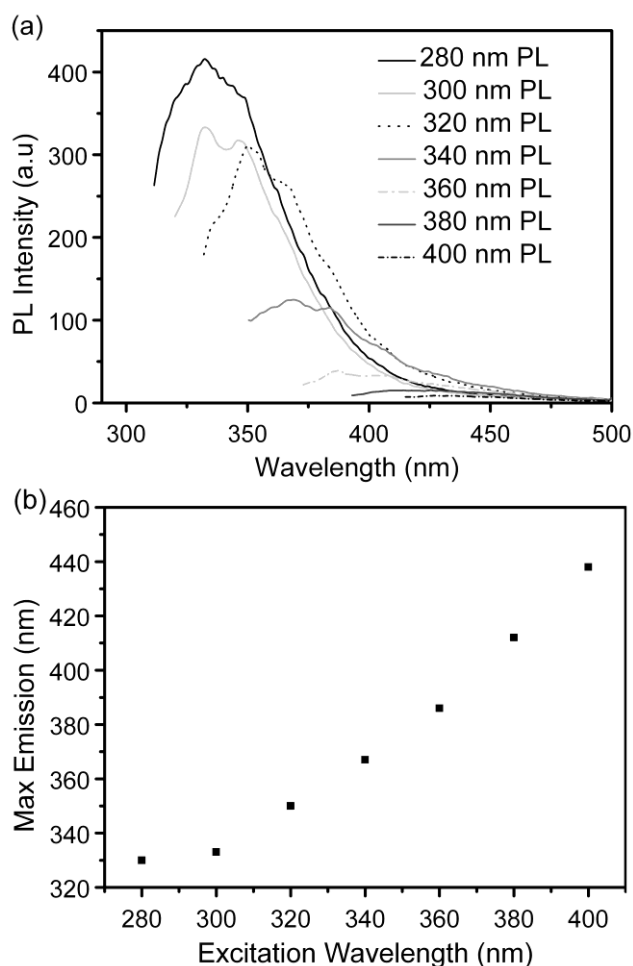


Figure 5. (a) Photoluminescence spectra of 1.9 nm silicon nanocrystals recorded at different excitation wavelengths. (b) Wavelength position of the luminescence maximum as a function of excitation wavelength.

This corresponds to an overall red shift in the PL peak position of 108 nm, as the excitation wavelength is increased by 120 nm, see Figure 5(b). This marked dependency on excitation

wavelength has been widely reported for silicon nanocrystals, prepared using different synthetic methods and surface functionalities.^[18,26,27] PL excitation (PLE) spectra recorded using the excitation wavelengths from 280 to 400 nm shown in Figures S.5 of the Supporting Information. Several closely spaced discrete features appear in the PLE spectra, with optimal excitation wavelengths still significantly above the energy of the absorption edge (3.5 eV). The PLE spectra are seen to decrease in intensity and red-shift in position when recording at longer emission wavelengths, again suggesting a combination of factors involving the nanocrystal core and the surface states.

This wavelength dependence is usually attributed to sample polydispersity, with the smaller NCs being selectively excited at shorter wavelengths, and larger NCs at longer wavelengths.^[27,28] However, the narrow size distributions in the Si NCs reported here precludes the shift in peak position being caused by polydispersity.^[14,26] Considering that the optimal excitation energies are considerably greater than the band gap energy, the sharp decrease in PL intensity at excitation wavelengths close to the absorption edge, the most plausible interpretation is that excitation at shorter wavelengths results in efficient generation of excitons, which readily transfer to and recombine at shallow surface trap states to give blue emission. Excitation at longer wavelengths may result in less efficient generation of excitons, which transfer to deeper trap states, resulting in less intense emission. There may also be increased transfer of excitons to nonradiative centers,^[25] which would also contribute to the overall decrease in PL intensity.

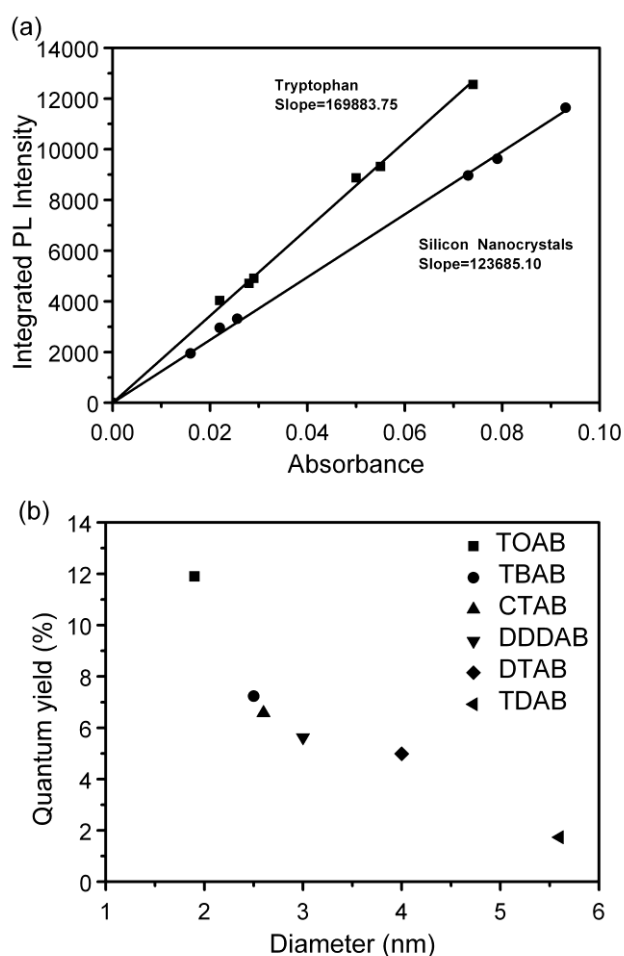


Figure 6. (a) Integrated PL intensity versus absorbance for various dilute dispersions of 1.9 nm diameters Si NCs in hexane and aqueous solutions of tryptophan (pH 7.0) recorded under identical excitation conditions. (b) Quantum yields of the Si NCs versus average core diameter.

It was shown in Figure 4 above that the photoluminescence intensity of the Si NCs decreases monotonically with increasing nanocrystal diameter. Photoluminescent quantum yields were determined using tryptophan as a reference emitter, see Experimental Section. Figure 6(a) shows the integrated PL intensity (280 nm excitation) of diluted dispersions of 1.9 nm diameters Si NCs in hexane and aqueous solutions of tryptophan (pH 7.0) recorded under identical excitation conditions. Linear regression analysis was employed to determine the relative PL intensities of the sample and reference solutions over the range of concentrations, see also Figure S.7 and Table S.2 for plots and analysis of Si NCs synthesized using the other

various surfactants. Figure 6(b) shows the calculated quantum yields of the Si NCs plotted against average core diameter. The quantum yield of the 1.9 nm Si NCs was found to be 12% at the optimal excitation wavelength of 280 nm, comparable with values reported for Si NCs of similar sizes reported in the literature.^[16,29] The quantum yields of the Si NCs exhibit an inverse relationship with the mean NC diameter, decreasing to *ca.* 7% for 2.5 nm nanocrystals, with a minimum of less than 2% recorded for 5.8 nm NCs. The observed trend in the quantum yields of the Si NCs may be accounted for by a combination of less efficient generation of excitons and the presence of greater number of nonradiative traps and recombination pathways with increasing size.

3. Conclusions

Size monodisperse silicon nanocrystals have been synthesized using a simple, room-temperature microemulsion synthesis method, with well-defined core diameters controlled between 2 to 6 nm by variation of the cationic quaternary ammonium salts used to form the inverse micelles. TEM imaging confirmed that the NCs are highly crystalline with a narrow size distribution, while the crystal structure of Si was confirmed by selected area electron diffraction (SAED). FTIR confirmed that each of the different sized nanocrystals possessed the same surface chemistry, with minimal surface oxidation. UV-Vis and PL spectroscopy showed significant quantum confinement effects, with moderate absorption in the UV spectral range, and a strong blue emission with a marked dependency on excitation wavelength. Determination of the photoluminescence quantum yield (Φ) of the Si NCs showed an inverse relationship with the NC core diameter, with a maximum of 12% measured for 2 nm NCs.

4. Experimental Section

Chemical Synthesis & Purification of Silicon Nanocrystals: The synthesis of the silicon nanocrystals (Si NCs) was adapted from the method reported by Tilley and co-workers.^[12] All reagents and solvents were purchased from Sigma-Aldrich Ltd. and used as received. In an inert atmosphere glove-box, 2.74 mmol of the surfactant was dissolved in 100 mL anhydrous toluene. 0.1 mL (0.87 mmol) SiCl₄ was then added to the solution and left to stir for 30 min. Si NCs were formed by the dropwise addition of 6 mL of 1 M lithium aluminum hydride in THF over a period of 2 min. CAUTION: Small amounts of silane gas, which is pyrophoric, could be evolved at this stage of the reaction and care should be taken to prevent exposure to air.^[11b] The solution was then left to react for 2.5 h. The excess reducing agent was then quenched with the addition of 60 mL methanol, upon which the dispersion became transparent. At this stage of the reaction the Si NCs are terminated by hydrogen and encapsulated within the inverse micelle.

Chemically passivated nanocrystals were formed by modifying the silicon-hydrogen bonds at the surface *via* the addition of 200 μ L of a 0.1 M H₂PtCl₆ in isopropyl alcohol as a catalyst, followed by 6 mL of 1-heptene. After stirring for 2.5 h, the Si NCs were removed from the glove box and the organic solvent removed by rotary evaporation. The resulting dry powder (consisting mainly of surfactant) was then redispersed in 20 mL hexane and sonicated for 30 min. The solution was then filtered twice using PVDF membrane filters (MILLEX-HV, Millipore, 0.45 μ M) to remove the surfactant, after which it was washed with 100 mL of n-methyl formamide (4 times) and then with distilled water. Alkyl-terminated Si NCs remain in the hexane phase. The Si NCs were further purified by chromatography. The solution was concentrated down to 1 mL and put into the column (1 cm, 41.0 cm). Sephadex gel LH-20 was used as the stationary phase. Fractions were collected every 50 drops at a flow rate of one

drop every 5 s. A hand held UV lamp (365 nm) was used to check each fraction for Si NCs luminescence. The fractions were then combined and concentrated down to 1 mL.

Characterization of Silicon Nanocrystals: UV-Vis absorption spectra were recorded using a Shimadzu UV PC-2401 spectrophotometer equipped with a 60 mm integrating sphere (ISR-240A, Shimadzu). Absorption spectra were recorded at room temperature using a quartz cuvette (1 cm) and corrected for the solvent absorption. Photoluminescence spectra of the Si NCs were recorded using a Perkin Elmer LS 50 luminescence spectrophotometer equipped with a pulsed Xenon discharge lamp. Quantum yields (QY) were measured using the comparative method described by Williams *et al.*^[30] Dilute dispersions of the Si NCs in hexane were prepared with optical densities between 0.01 - 0.1 and compared against aqueous tryptophan solutions with similar optical densities as reference emitters. The quantum yield of the tryptophan reference was corrected for temperature using the model described by Robbins *et al.*, see Supporting Information.^[31] PL spectra of all the Si NCs and tryptophan solutions were acquired using an excitation wavelength of 280 nm, and the total PL intensity integrated over 300-475 nm. Linear regression analysis was employed to determine the relative PL intensities of the sample and reference solutions over the range of concentrations, allowing the quantum yield of the Si NCs; see Supporting Information. FT-IR spectra were recorded on a Bio Rad Excalibur FTS 3000 spectrometer in steps of 1 cm⁻¹ and averaging scans. Samples were formed by placing an aliquot of silicon crystals dispersed in hexane onto 32 mm round, 3 mm thick, drilled NaCl plates, after which the sample was allowed to evaporate to dryness. X-ray photoelectron spectroscopy (XPS) measurements were carried out using a Kratos Axis-165 photoelectron spectrometer. The narrow scan spectra were obtained under high vacuum conditions by using a monochromatic Al K α x-ray radiation at 15 kV and 10 mA with a analyzer pass energy of 20 eV. Substrates were cleaned for 20 min in piranha solution, rinsed with water and dried with nitrogen. A few drops of the Si NC solution dissolved in

chloroform were dropped on a clean gold surface substrate. All spectra were acquired at room temperature and binding energies were referenced to the Au 4f_{7/2} line. All spectra were fitted with three peaks using a Shirley background. Transmission electron microscopy (TEM) images and selective area electron diffraction patterns (SAED) were acquired using a high-resolution JEOL 2100 electron microscope, equipped with a LAB₆ electron source and Gatan DualVision 600 Charge-Coupled Device (CCD), operating at an accelerating voltage of 200 keV. Energy dispersive x-ray spectra (EDS) spectra were recorded on using an Oxford INCA x-sight detection spectrometer. Spectra were obtained from an area of the grid where there was a large amount of NCs. A process time of 3-4 seconds was used and the spectra obtained using an integration time of 40 s. TEM samples were prepared by depositing 300 µl of Si NC dispersion, onto a holey carbon coated TEM grid (400-mesh, #S147-3H, Agar Scientific). Particle size analysis of TEM images was carried out using the Particle Size Analyzer macro (r12, freely available online at <http://code.google.com/p/psa-macro/>) running on Image J software.

Acknowledgements

This work was supported by the European Commission under the FP7 Projects SNAPSUN (grant agreement n° 246310) and CommonSense (grant agreement n° 261809) and the Irish Higher Education Authority under the PRTL I programs (Cycle 3 “Nanoscience” and Cycle 4 “INSPIRE”). The authors would like thank to Dr. Fathima Laffir at the Materials and Surface Science Institute, Limerick, for performing the XPS measurements.

References

- [1] a) M. Green, *Angew. Chem., Int. Ed.* **2004**, *43*, 4129; M. Green, *Angew. Chem.* **2004**, *116*, 4221; b) M. Bruchez, M. Moronne, P. Gin, S. Weiss, A. P. Alivisatos, *Science* **1998**, *281*, 2013; c) P. O. Anikeeva, J. E. Halpert, M. G. Bawendi, V. Bulovic, *Nano Lett.* **2009**, *9*, 2532; d) S. Coe, W.-K. Woo, M. Bawendi, V. Bulovic, *Nature* **2002**, *420*, 800.
- [2] a) M. L. Mastronardi, F. Maier-Flaig, D. Faulkner, E. J. Henderson, C. Kübel, U. Lemmer, G. A. Ozin, *Nano Lett.* **2012**, *12*, 337; b) M. J. Llansola Portolés, R. Pis Diez, M. L. Dell'arciprete, P. Caregnato, J. J. Romero, D. O. Mártire, O. Azzaroni, M. Ceolín, M. C. Gonzalez, *J. Phys. Chem. C* **2012**, *116*, 11315.
- [3] S. Perraud, E. Quesnel, S. Parola, J. Barbé, V. Muffato, P. Faucherand, C. Morin, K. Jarolimek, R. A. C. M. Van Swaaij, M. Zeman, S. Richards, A. Kingsley, H. Doyle, K. Linehan, S. O'Brien, I. M. Povey, M. E. Pemble, L. Xie, K. Leifer, K. Makasheva, B. Despax, *Phys. Status Solidi A* **2013**, *210*, 649.
- [4] a) V. Kapaklis, C. Politis, P. Pouloupoulos, P. Schweiss, *Appl. Phys. Lett.* **2005**, *87*, 123114; b) S. - M. Liu; S. Sato; K. Kimura, *Langmuir* **2005**, *21*, 6324.
- [5] a) S. Sato, M. T. Swihart, *Chem. Mater.* **2006**, *18*, 4083; b) F. Hua, M. T. Swihart, E. Ruckenstein, *Langmuir* **2005**, *21*, 6054.
- [6] a) L. T. Canham, *Appl. Phys. Lett.* **1990**, *57*, 1046; b) G. Belomoin, J. Therrien, M. Nayfeh, *Appl. Phys. Lett.* **2000**, *77*, 779; c) J. H. Ahire, Q. Wang, P. R. Coxon, G. Malhotra, R. Brydson, R. Chen, Y. Chao, *ACS Appl. Mater. Interfaces* **2012**, *4*, 3285.
- [7] a) J. D. Holmes, K. J. Ziegler, R. C. Doty, L. E. Pell, K. P. Johnston, B. A. Korgel, *J. Am. Chem. Soc.* **2001**, *123*, 3743; b) D. S. English, L. E. Pell, Z. Yu, P. F. Barbara, B. A. Korgel, *Nano Lett.* **2002**, *2*, 681.
- [8] a) J. Zou, R. K. Baldwin, K. A. Pettigrew, S. M. Kauzlarich, *Nano Lett.* **2004**, *4*, 1181; b) D. Neiner, H. W. Chiu, S. M. Kauzlarich, *J. Am. Chem. Soc.* **2006**, *128*, 11016.

- [9] A. Shiohara, S. Prabakar, A. Faramus, C.-Y. Hsu, P.-S. Lai, P. T. Northcote, R. D. Tilley, *Nanoscale* **2011**, *3*, 3364.
- [10] a) M. - P. Pileni, *Nat. Mater.* **2003**, *2*, 145; b) M. - P. Pileni, *J. Exp. Nanosci.* **2006**, *1*, 13.
- [11] a) J. P. Wilcoxon, G. A. Samara, P. N. Provencio, *Phys. Rev. B* **1999**, *60*, 2704. b) D. L. Huber, J. P. Wilcoxon, G. A. Samara, *Appl. Phys. Lett.* **1999**, *74*, 3164.
- [12] R. D. Tilley, J. H. Warner, K. Yamamoto, I. Matsui, H. Fujimori, *Chem. Commun.* **2005**, 1833.
- [13] M. Rosso-Vasic, L. De Cola, H. Zuilhof, *J. Phys. Chem. C* **2009**, *113*, 2235.
- [14] A. Shiohara, S. Hanada, S. Prabakar, K. Fujioka, T. H. Lim, K. Yamamoto, P. T. Northcote, R. D. Tilley, *J. Am. Chem. Soc.* **2010**, *132*, 248.
- [15] a) J. Wang, S. Sun, F. Peng, L. Cao, L. Sun, *Chem. Commun.* **2011**, *47*, 4941; b) X. Cheng, R. Gondosiswanto, S. Ciampi, P. J. Reece, J. J. Gooding, *Chem. Commun.* **2012**, *48*, 11874.
- [16] M. Rosso-Vasic, E. Spruijt, B. Van Lagen, L. De Cola, H. Zuilhof, *Small* **2008**, *4*, 1835.
- [17] Y. Chao, L. Šiller, S. Krishnamurthy, P. R. Coxon, U. Bangert, M. Gass, L. Kjeldgaard, S. N. Patole, L. H. Lie, N. O'Farrell, T. A. Alsop, A. Houlton, B. R. Horrocks, *Nat. Nanotechnol.* **2007**, *2*, 486.
- [18] J. H. Warner, H. Rubinsztein-Dunlop, R. D. Tilley, *J. Phys. Chem. B* **2005**, *109*, 19064.
- [19] M. Rosso-Vasic, E. Spruijt, B. Van Lagen, L. De Cola, H. Zuilhof, *Small* **2009**, *5*, 2637.
- [20] M. Dasog, Z. Yang, S. Regli, T. M. Atkins, A. Faramus, M. P. Singh, E. Muthuswamy, S. M. Kauzlarich, R. D. Tilley, J. G. C. Veinot, *ACS Nano* **2013**, *7*, 2676.

- [21] C.-S. Yang, R. A. Bley, S. M. Kauzlarich, H. W. H. Lee, G. R. Delgado, *J. Am. Chem. Soc.* **1999**, *121*, 5191.
- [22] J. G. C. Veinot, *Chem. Commun.* **2006**, 4160.
- [23] N. Shirahata, *Phys. Chem. Chem. Phys.* **2011**, *13*, 7284.
- [24] A. Sa'ar, *J. Nanophotonics* **2009**, *3*, 032501.
- [25] S. Yang, W. Li, B. Cao, H. Zeng, W. Cai, *J. Phys. Chem. C* **2011**, *115*, 21056.
- [26] Z. Ding, B. M. Quinn, S. K. Haram, L. E. Pell, B. A. Korgel, A. J. Bard, *Science* **2002**, *296*, 1293.
- [27] S. Pradhan, S. Chen, J. Zou, S. M. Kauzlarich, *J. Phys. Chem. C* **2008**, *112*, 13292.
- [28] J. R. Siekierzycka, M. Rosso-Vasic, H. Zuilhof, A. M. Brouwer, *J. Phys. Chem. C* **2011**, *115*, 20888.
- [29] a) S.-W. Lin, D.-H. Chen, *Small* **2009**, *5*, 72; b) J. H. Warner, A. Hoshino, K. Yamamoto, R. D. Tilley, *Angew. Chem., Int. Ed.* **2005**, *44*, 4550; J. H. Warner, A. Hoshino, K. Yamamoto, R. D. Tilley, *Angew. Chem.* **2005**, *117*, 4626.
- [30] A. T. R. Williams, S. A. Winfield, J. N. Miller, *Analyst* **1983**, *108*, 1067.
- [31] R. J. Robbins, G. R. Fleming, G. S. Beddard, G. W. Robinson, P. J. Thistlethwaite, G. J. Woolfe, *J. Am. Chem. Soc.* **1980**, *102*, 6271.

Received: ((will be filled in by the editorial staff))

Revised: ((will be filled in by the editorial staff))

Published online on ((will be filled in by the editorial staff))

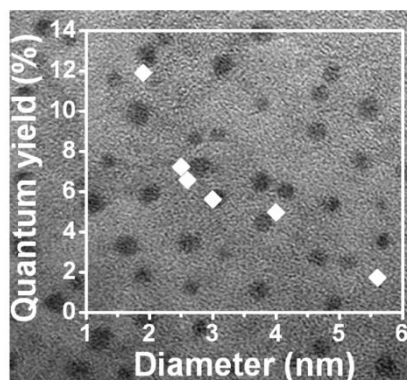
The table of contents entry

Highly monodisperse Si NCs (2 – 6 nm) are synthesized by solution-phase reduction of SiCl₄ within inverse micelles. Alkyl-terminated NCs with mean diameters from 2 to 6 nm are produced by varying the cationic surfactants used, confirmed by TEM and FTIR. Si NCs exhibit strong blue emission, with a highest quantum yield of 12 % for the smallest NCs.

Silicon nanocrystals

K. Linehan and H. Doyle*

Size Controlled Synthesis of Silicon Nanocrystals using Cationic Surfactant Templates



Page Headings

Left page: Linehan et al.

Right page: Size Controlled Synthesis of Silicon Nanocrystals

Supporting Information:

Size Controlled Synthesis of Silicon Nanocrystals using Cationic Surfactant Templates

*Keith Linehan and Hugh Doyle**

Tyndall National Institute, University College Cork, Lee Maltings, Cork, Ireland.
E-mail: hugh.doyle@tyndall.ie

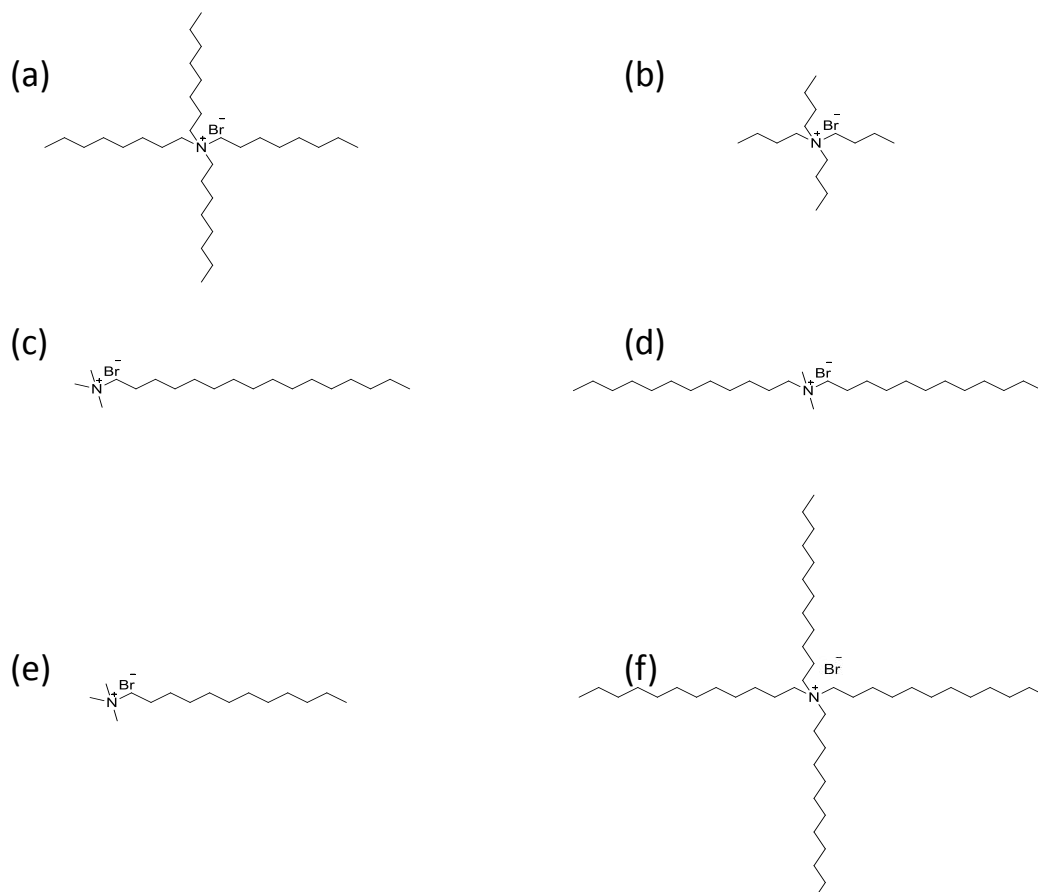


Figure S.1. Molecular structure of the different surfactants (a) Tetraoctyl ammonium bromide (b) Tetrabutyl ammonium bromide (c) Cetyltrimethyl ammonium bromide (d) Didodecyl dimethyl ammonium bromide (e) Dodecyltrimethyl ammonium bromide (f) Tetradodecyl ammonium bromide.

<i>d</i> spacing calculated from SAED, Å	<i>d</i> spacing in bulk Si, ^{SI} Å	(hkl) assignment
3.14	3.13	(111)
1.92	1.92	(220)
1.68	1.63	(311)
1.31	1.35	(400)

Table S.1. *d* spacing calculated from selected area electron diffraction of the silicon nanocrystals.

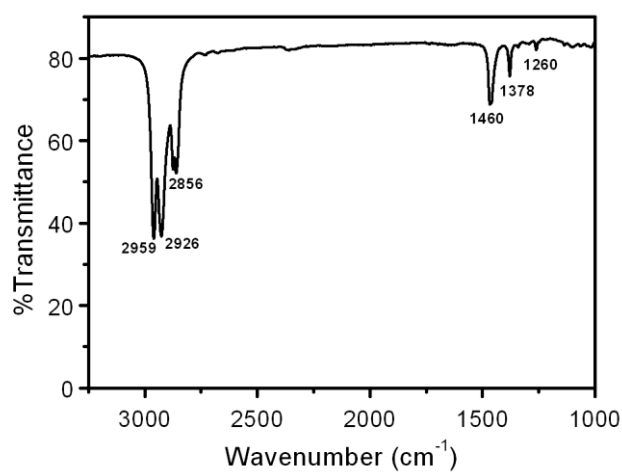


Figure S.2. Fourier transform infrared spectrum of alkyl-terminated silicon nanocrystals using TOAB as the surfactant.

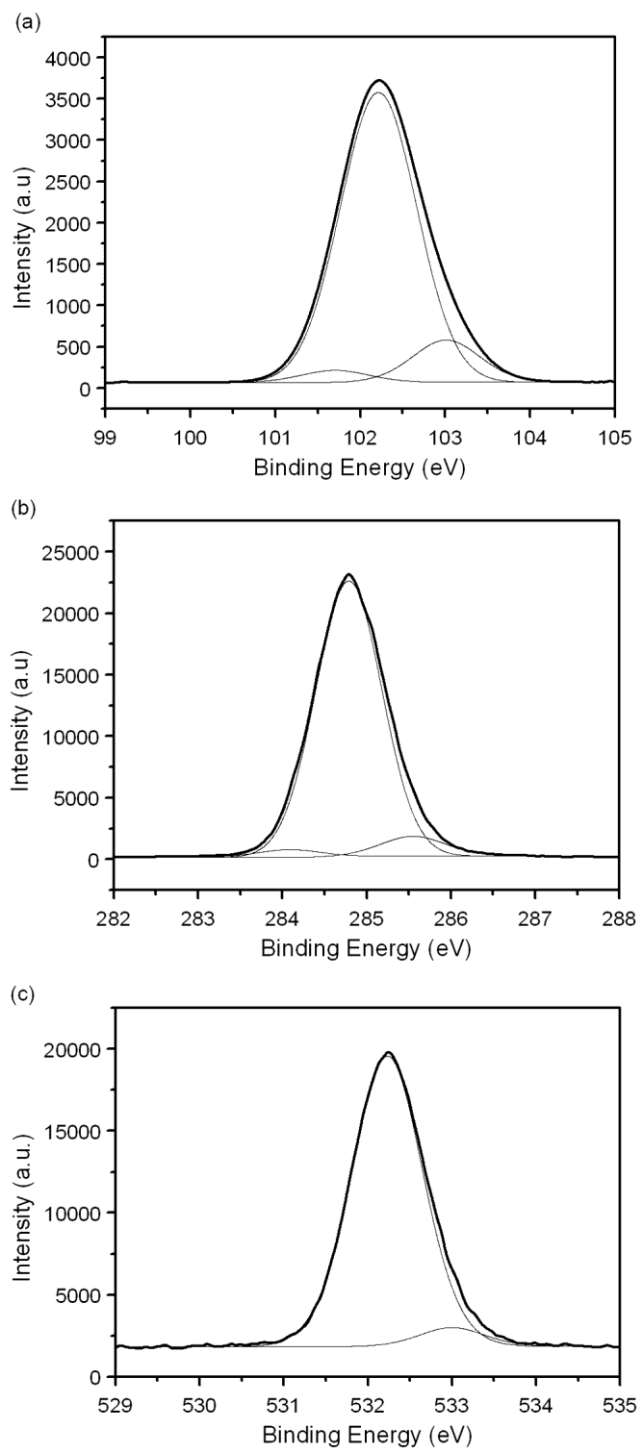


Figure S.3. XPS spectra of alkyl-terminated silicon nanocrystals.

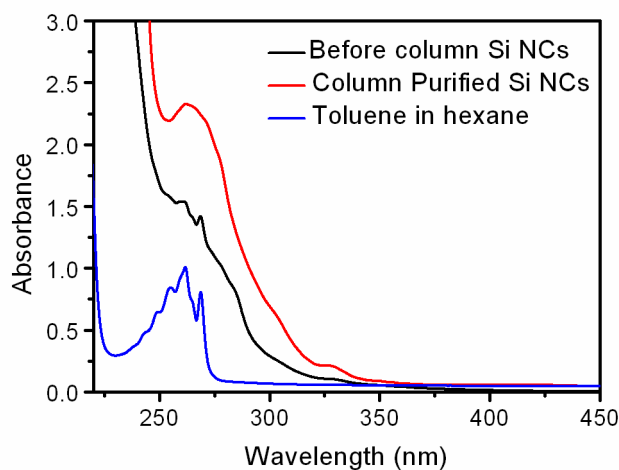


Figure S.4. UV-Vis absorbance spectra of the as-synthesized silicon nanocrystals (black lines), column purified silicon nanocrystals (red lines), and dilute solution of toluene in hexane (blue lines).

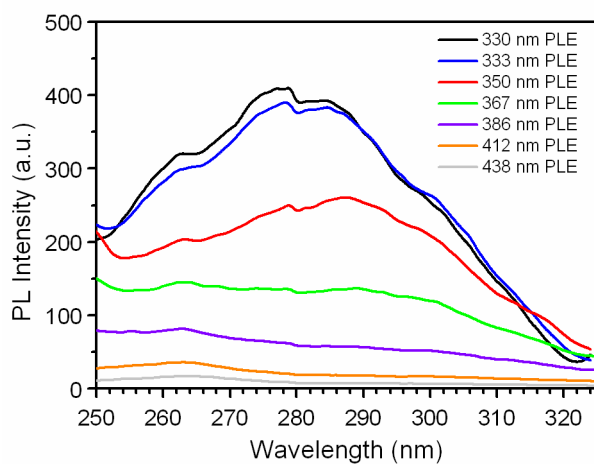


Figure S.5. Photoluminescence excitation (PLE) spectra of 1.9 nm silicon nanocrystals. Wavelength positions refer to maximum emission positions shown in Figure 5(b).

Calculation of Quantum Yield of Tryptophan as a function of temperature

The fluorescence standard tryptophan was selected as the reference material as 98% of its luminescence spectrum overlaps that of the silicon nanocrystals. The QY of tryptophan is dependent on the temperature, pH, concentration and solvent. Robbins *et al.* previously determined the temperature dependence of the tryptophan QY at pH 7.^[S2] The fluorescence lifetime (τ^{-1}) of tryptophan at pH 7 is expressed as:

$$\tau^{-1}(pH\ 7) = k_f + k_t + k_{e_{aq}^-} + k_i$$

Where k_f is the fluorescence, k_t is intersystem crossing, $k_{e_{aq}^-}$ is photoionization and k_i is intramolecular quenching. The work carried out by Robbins *et al.* was replicated to calculate the quantum yield of tryptophan at any temperature. Figure S6 shows the modeling of the dependence of the QY of tryptophan on temperature for all the different processes involved at pH 7. From the data, the QY of fluorescence, at a certain temperature can be determined and therefore the QY of the silicon NCs can be calculated extremely accurately.

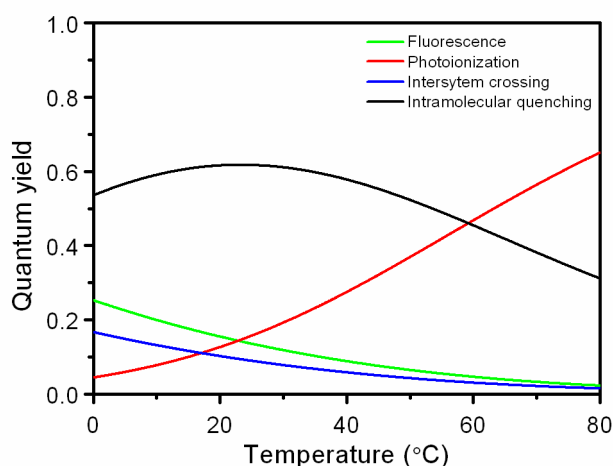


Figure S.6. Calculated quantum yields of fluorescence, intersystem crossing, photoionization and intramolecular quenching for tryptophan at pH 7, as a function of temperature.

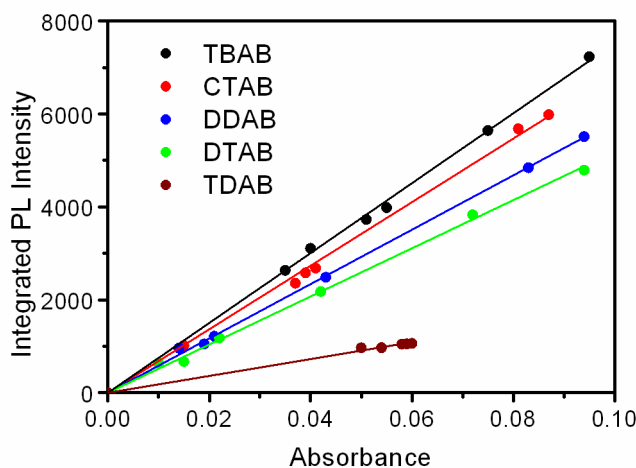


Figure S.7. Integrated PL intensity versus absorbance for dilute dispersions of silicon nanocrystals synthesized using different surfactants in hexane.

Surfactant	Slopes	Quantum Yield (Φ)
TBAB	75168.74	7.2
CTAB	68372.39	6.6
DDAB	58491.82	5.6
DTAB	51828.39	5.0
TDAB	17939.17	1.7

Table S.2. Fitted slopes and calculated quantum yields from linear regression analysis of data shown in Figure S.7 above.

References

- [S1] I. N. Germanenko, M. Dongol, Y. B. Pithawalla, M. Samy El-Shall, J. A. Carlisle, *Pure Appl. Chem.* **2000**, *72*, 245–255, 2000.
- [S2] R. J. Robbins, G. R. Fleming, G. S. Beddard, G. W. Robinson, P. J. Thistlethwaite, G. J. Woolfe, *J. Am. Chem. Soc.* **1980**, *102*, 6271.